Enhancement in Efficiency and Optoelectronic Quality of Perovskite Thin Films Annealed in MACl Vapor

Dhruba B. Khadka† Yasuhiro Shirai†,* Masatoshi Yanagida,† Takuya Masuda† and Kenjiro Miyano†

†Global Research Center for Environment and Energy based on Nanomaterials Science (GREEN), National Institute for Materials Science (NIMS), 1-1 Namiki, Tsukuba, Ibaraki 305-0044, Japan.

Corresponding Author

*E-mail: SHIRAI.Yasuhiro@nims.go.jp

ABSTRACT

We analyzed and compared quantitatively the optoelectronic characteristics of perovskite PV devices with and without annealing the perovskite layer in methyl ammonium chloride vapor atmosphere (MACl treatment). We found that the MACl treatment resulted in the mitigation of defect states, reduced defect density, improvement in carrier profile, and passivation of recombination activities, which we infer as natural consequences of significantly improved film quality with better crystallinity and grain morphology of the perovskite layer. MACl treated devices are more efficient with the best efficiency of ~15.1% with small standard deviation (std) (0.50%) and improved stability compared to devices without MACl annealing of best efficiency of 12.4% with std of 0.66%.

Keywords: Perovskite, MACl treatment, recombination, defect state, solar cell.

1. Introduction

Metal halide perovskite based solar cells have emerged with the startling progress in device efficiencies leaping from 3.8% to the current record of 22.1% within short time span in the photovoltaic research record.[1-3] This was led by the excellent optoelectronic properties of perovskite materials such as high absorption in the visible range,[4] ambipolar charge carriers,[5] small exciton binding energy,[6] long charge carrier diffusion length[7, 8] and band gap tunability.[9-11] A number of efforts have been reported to optimize the device performance, e.g., various fabrication techniques[12-16] together with different crystallization approaches[17-19] and tailoring the device architecture with different electron and hole transport layers.[20-22] Despite the remarkable progress, the current-voltage (J-V) hysteresis, fluctuation of power conversion efficiency (PCE), and instability remain issues to be resolved.[23-25] The hysteresis problem may be solved by adjusting the electron/hole transport layers (ETL/HTL).[26, 27] On the other hand, the scattering in device performances, control of optoelectronic properties, and instability of the devices still remain.[13, 24, 25, 27] There is much room to address these issues[24, 25, 28] by focusing on getting high quality perovskite films, passivation of defect, and control of spurious ionic migration and diffusion phenomena.

It has been widely observed that the performances of perovskite solar cells (PVSCs) are strongly influenced by the surface morphology, crystallinity, and grain growth of the perovskite films.[17, 18, 29, 30] In order to get high quality perovskite films, various experimental approaches such as vacuum deposition,[14] solution processes[13, 15-18] and vapor assisted solution processes[31] have been adopted. Being easy and cost effective with promising track record of progress, the solution processes have been broadly adopted and intensively investigated, in which many paths to better quality perovskite films have been explored, e.g., by varying the processing conditions,[12, 16, 29] solvent engineering,[17] mixed or hybrid precursors,[13, 32-35] fast deposition crystallization[36] and incorporating various additives.[37, 38]

In addition to the film preparation process, post deposition treatment (PDT) has also been reported to be equally beneficial to control the morphology and crystallinity of perovskite films and hence device performance.[39-44] The major PDT techniques have been the thermal treatment,[16] solvent annealing[17, 18] and methylamine-gas treatment.[19] Because of its simplicity, thermal treatment is often applied to assist the formation of perovskite phase with enhanced crystallinity and morphology, and to remove by-products.[39, 40] The annealing temperature and duration are crucial to get optimized morphology. The solvent annealing has been also widely employed to improve the morphology and crystallinity of the films.[18, 41-43] In this approach, the vapor of solvents such as DMF, DMSO etc. having high solubility to lead iodide and methyl ammonium iodide (MAI) provides a "wet atmosphere" so that the ionic or molecular constituents could easily diffuse in the film, promoting the grain growth resulting in the grain sizes comparable or larger than the film thickness.[18,42] The larger grain size and better crystallinity lead to reduction of the number of the grain boundaries and defects, which are prerequisites for enhancement in device efficiency.

Here, we introduce a simple PDT approach, i.e., annealing of the perovskite films together with the MACl powder in a closed vessel (**Figure 1**). We hereafter refer to it as "MACl treatment". This requires no handling of solvents or gaseous materials that often require laborious experimental setups to avoid contamination of the working environments and for safety. We found that the MACl treatment can significantly improve the optoelectronic properties of the films and device performances. The lowest sublimation temperature (195 ℃) (or enthalpy of sublimation (78 kJ mol^{-1}) of MACl among halide derivatives[45] ensures sufficient MACl vapor partial pressure even at around 100 °C, the usual perovskite annealing temperature. We speculate that the excess MACl vapor compensates loss of methyl ammonium and the additional chlorine is beneficial for crystallization and improvement of film quality[46] because introducing chlorine in fabrication process with mixed chloride/iodide perovskite precursor is

reported to result in better perovskite film quality and to improve the carrier transport characteristics.[17, 47-49]

The MACl treatment allowed us to achieve the champion PCE of 15.1% with narrow standard deviation of ±0.5% with average PCE of 14.4% over 60 devices fabricated at five different batches, giving better reproducibility and stability of the devices with reference to our earlier reports.[27,50] We also performed the device simulation using solar cell capacitor simulator called SCAPS to illustrate impact of the MACl treatment on the device performance.

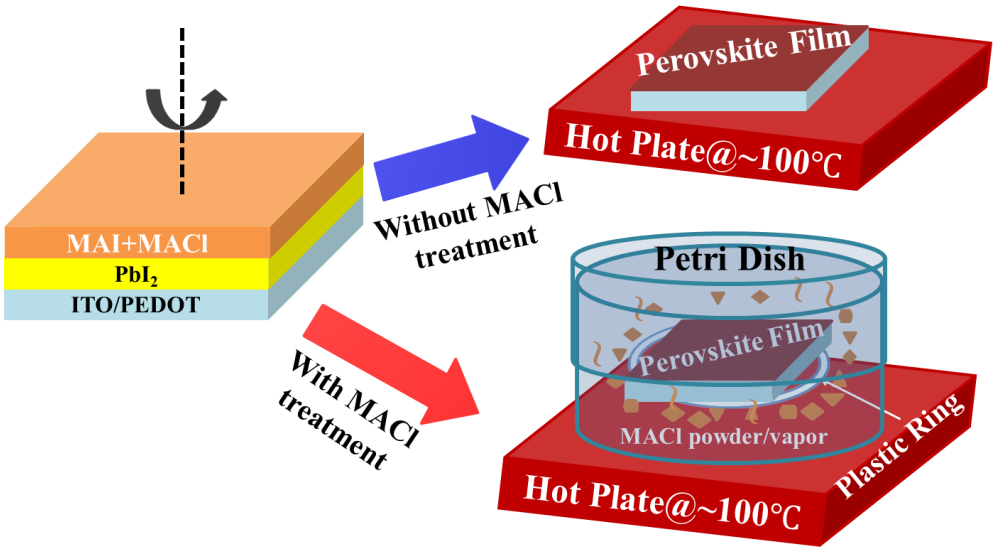

Figure 1. Schematic illustration of experimental approach with or without MACl treatment.

2. Results and Discussions

The crystal quality and structural evolution of perovskite thin films were investigated by XRD patterns as depicted in **Figure 2**. The XRD pattern of PbI_2 thin film (Figure 2a) showed a well-defined characteristic structure of PbI_2 with dominant orientation assigned to (001), (101) and (003)[12, 31] whereas that of as-deposited perovskite film formed by just spin coating of MACl+ MAI mixed precursor on PbI_2 layer revealed perovskite film grown with moderate crystal quality with dominant crystal orientation assigned to (110) along with trace signal from PbI_2

as depicted in Figure 2b. The XRD patterns of perovskite films with or without MACl treatment (Figure 2c, d) showed identical characteristic XRD patterns with enhanced crystal orientation peaks assigned to (110), (112), (211), (202), (220), and (310) of lead halide perovskite phase.[8, 31, 41] Furthermore, the perovskite film with MACl treatment (Figure 2d) exhibits more enhanced XRD pattern than that of perovskite film without MACl treatment, which indicates improvement in crystal quality. To have further evaluation of crystal quality, we also calculated the crystallite size (L) by using Scherrer's formula,[51] $L= \frac{0.9\lambda}{\beta \cos\theta}$, where λ is wavelength of X- ray and β denotes the full width at half maximum (FWHM) of the diffraction peak. The average crystallite sizes of as-grown perovskite film and perovskite films with and without MACl treatment were estimated to be approximately 35.8, 50.2 and 96.5 nm, respectively, which also supports the improvement in film quality as a consequence of MACl treatment.

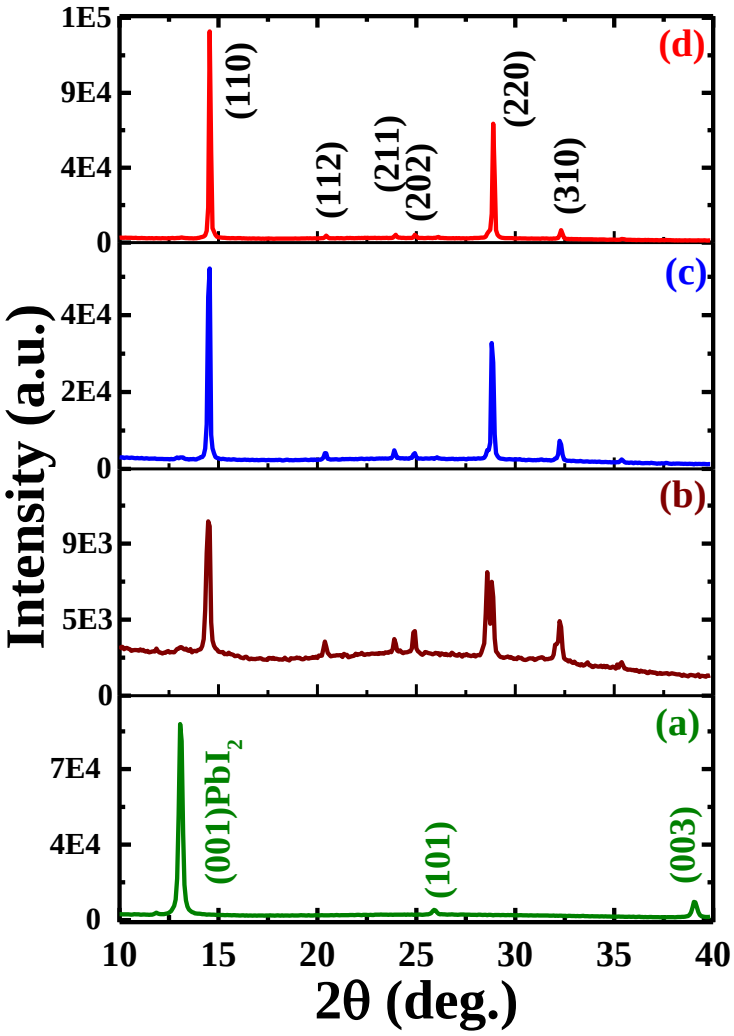

Figure 2. XRD patterns of (a) PbI_2 film (b) as- deposited perovskite film, perovskite films followed by (c) no MACl treatment and (d) MACl treatment.

The top view of the perovskite films with and without MACl treatment, as depicted in **Figure 3**, illustrates distinct surface morphology. The surface morphology of PbI_2, as-grown perovskite, perovskite films with and without MACl treatment are shown in supporting information (Figure S1). The grain sizes are broadly distributed ranging from 80-500 nm with average of ~200 nm for perovskite films without MACl treatment whereas comparatively uniform grain sizes ranging from 150-500 nm with average of ~300 nm are observed for the perovskite films with MACl treatment, which agrees with the crystallite size estimated from XRD patterns and with the results of other reports.[17, 27, 50]

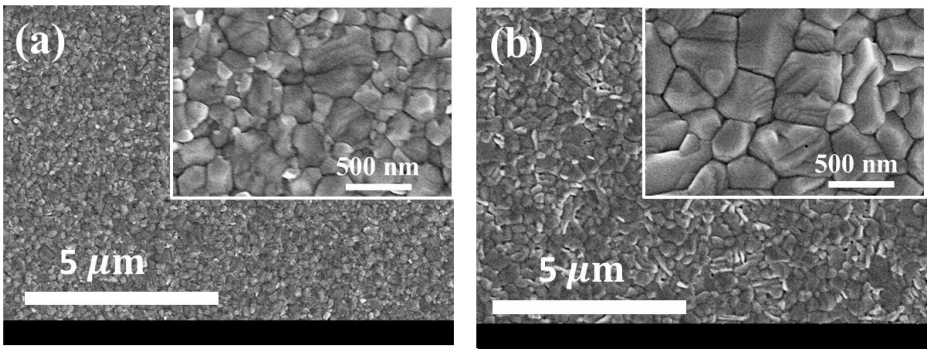

Figure 3. Top view SEM images of perovskite films ((a) without MACl treatment and (b) with MACl treatment [inset: magnified images].

We also studied the composition and distribution of constituent elements in fabricated films as shown in supporting information (Figures S2 and S3). No noticeable difference was found between the elemental compositions of the MACl treated films and that of the untreated films. In particular, no additional chlorine is incorporated in MACl treated films. This is in accordance with the well-matched XRD peaks of both types of films as depicted in Figure 2c, d. It indicates that the MACl treatment promotes the crystal quality without any additional elemental incorporation in perovskite film within the detection limit.

Furthermore, the perovskite films were characterized by XPS. We measured XPS spectra of perovskite film surface and the bulk by etching the film by ~80 nm as shown in supporting information (Figure S4). Although there is a dominant role played by MACl treatment on perovskite film quality, XPS characteristic feature of Cl 2p core was absent within the detection limit in accordance with the report by William et al.[49] The XPS characteristic features of I were found to be similar for both types of films. On the other hand, a distinct XPS characteristic feature pertaining to Pb was observed both on the surface and in the bulk of the perovskite films. As shown in Figures S4a6 and b6, the Pb peaks consist of two groups; the one with lower binding energy is assigned as Pb $4f_{7/2}$ and the higher one as Pb $4f_{5/2}$. The peaks at ~137.6 and

142.7 eV are attributed to Pb in perovskite structure.[52, 53] The additional small peaks around 135.7 and 141.9 eV marked with star (*) may be due to unsaturated Pb.[52]

These results consolidate that the MACl treatment promotes better crystallinity coupled with compact, uniform, large grains and better film quality without making any noticeable change in stoichiometric and elemental distribution in the perovskite films.

The photophysical properties of perovskite films were investigated by absorption and PL spectra. We have collected UV-Vis spectra of various films (Figure S5). The UV-VIS spectra (Figure S5c) of the perovskite films with and without MACl treatment are similar except for a slight difference in the UV region. This trend is unaffected by the addition of HTL and ETL. The UV-VIS spectra of PEDOT:PSS/perovskite and PEDOT:PSS/perovskite/PCBM layers (Figure S5d, e) are in accordance with Figure S5c when corrected for the absorption spectra of HTL and ETL, (Figure S5b). Figure 4a shows the room temperature PL spectra of respective perovskite films. The PL intensity of perovskite film with MACl treatment was drastically enhanced (~9 times) than that of films without MACl treatment. Furthermore, photoluminescence decay measurements (Figure 4b) after fitting with a biexponential function revealed average carrier lifetimes of 235 and 136 ns in perovskite films with and without MACl treatment, respectively. Those characteristic features of absorption, PL spectra, and PL decay are in good agreement with results reported by Zhang et al.[52] The enhancement in PL intensity and lifetime for perovskite films with MACl treatment is attributed to the improved crystallinity and larger grain sizes (Figure 3). Nonradiative recombination centers provide decay channels of free carriers and they are likely to be energetic disorders and active defects. The better crystallinity will contribute to reduce them in the bulk while the larger grain sizes reduce the grain boundary. Similar improvement was reported in perovskite films processed with hypophosphorous acid.[52]

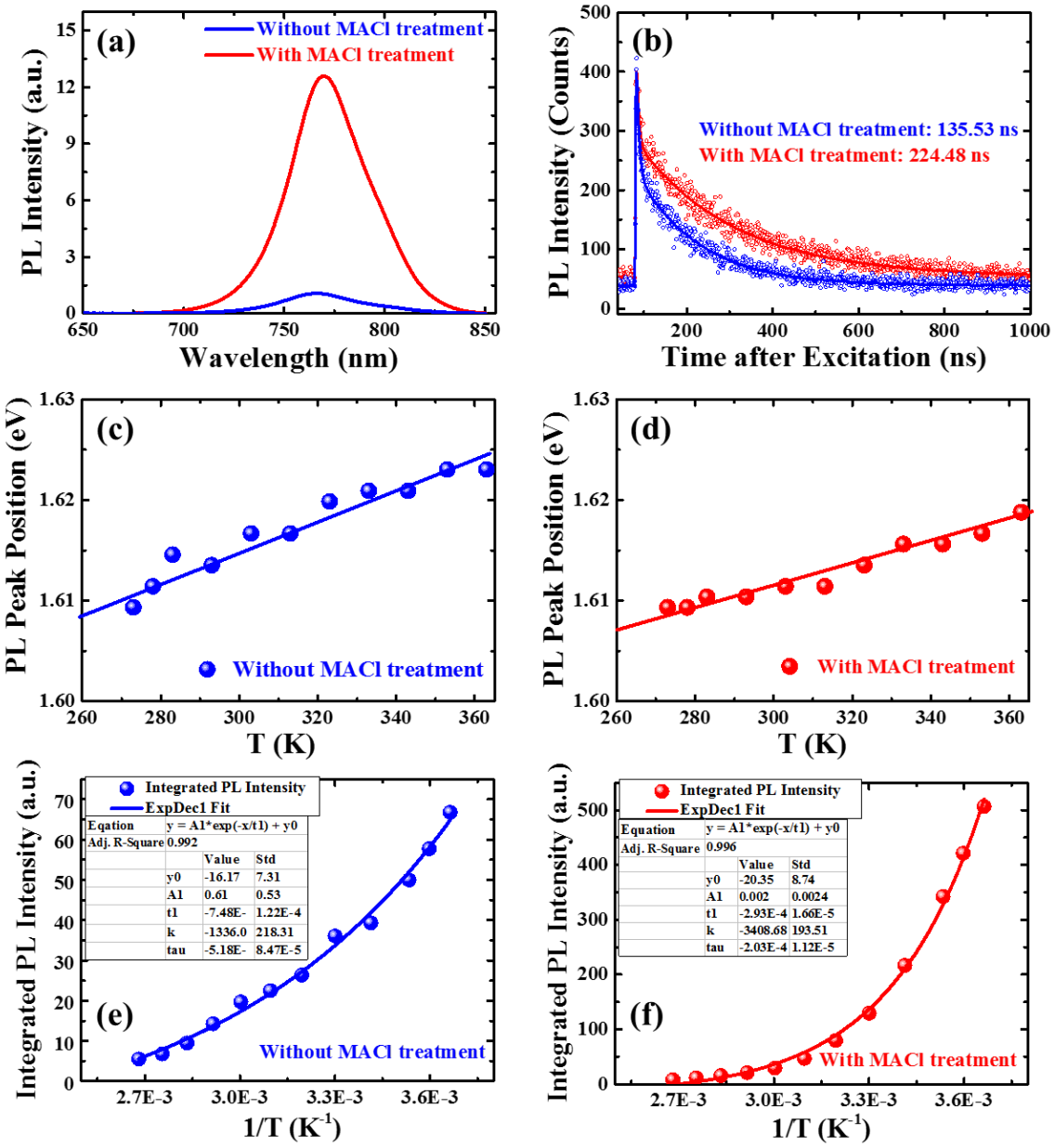

Figure 4. Photoluminescence (PL) spectra (a), and PL decay (b) of perovskite thin films with and without MACl treatment. The plots of temperature dependent PL peak position (c, d) and integrated PL intensity (e, f) of respective films. The temperature dependent PL spectra of perovskite films are depicted in Figure S6 (supporting information). Here, solid line in plots (c, d) represents linear fitting whereas that in plots (e, f) represents non-linear fitting. Inset Table in plots (e, f) are fitting parameters.

We also measured temperature dependent PL spectra of perovskite films from 273 to 373 K as depicted in Figure S6 (supporting information). With increase in temperature, we observed slight blue shift with faster broadening on the high energy side (Figure 4c, d), in close agreement with the previous reports.[54,55] We observed slightly different temperature dependence in films with and without MACl treatment in terms of the quenching trend of PL intensity (Figure S6a, b and Figure 4e, f). The temperature dependence of the PL peak position is $\frac{dE}{dT}$ = 0.103 $\pm$ 0.005 meV/K and 0.129 $\pm$ 0.015 meV/K for perovskite films with and without MACl treatment, respectively, which is analogous to the report by Wu et al.[54] These results collectively support the fact that the perovskite films with MACl treatment have better quality as a consequence of reduction or mitigation of defect states and recombination activities which will be further discussed in the later analysis.

Figure 5 depicts SEM cross-sectional images of samples having the layered structure ITO/ PEDOT:PSS/perovskite/PCBM/TBAI prior to silver electrode deposition to complete the device. The image of the MACl untreated film (Figure 5a) has mixed up features of grain sizes whereas that of the MACl treated film (Figure 5b) has comparatively well grown large grains extending between the electrodes, which is beneficial for effective carrier transport and hence efficient photovoltaic device.[14, 16, 18]

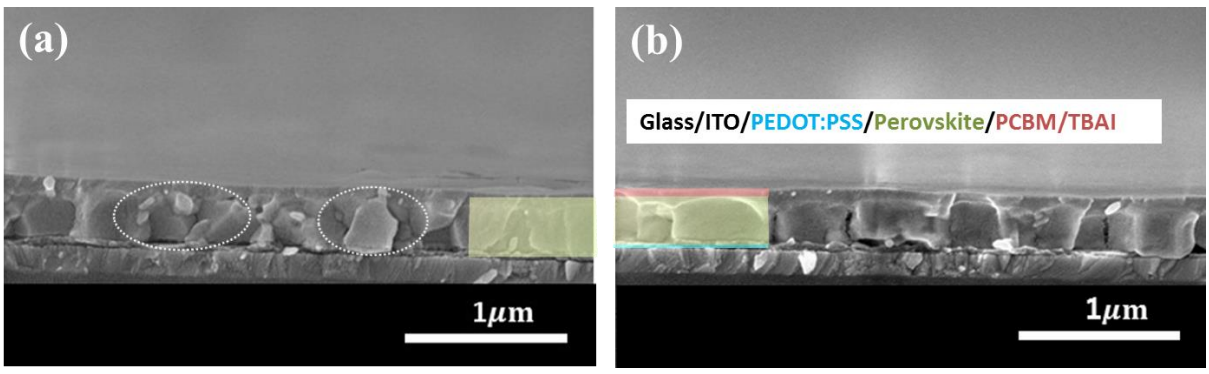

Figure 5. Cross-sectional SEM images of ITO/PEDOT:PSS/perovskite/PCBM/TBAI structure having perovskite thin films (a) without MACl treatment and (b) with MACl treatment.

In order to see the effect of the film quality on the carrier recombination, we studied and compared the photovoltaic performance of the complete devices fabricated with and without MACl treatment. The current density-voltage (J-V) characteristics and the spectral response of champion PVSCs with and without MACl treatment are shown in Figure 6a. The PCEs of the two types of devices are 15.1% and 12.4%, respectively. We emphasize that all devices were fabricated under exactly the same conditions except for the MACl treatment. The device parameters are summarized in Table 1. The enhancement in V_{OC}, FF and R_{Sh} for the MACl treated device over the untreated device is much better compared to the enhancement in J_{SC} and R_S. The values of FF and R_{sh} are comparable to the best reported.[12, 14, 18, 20, 33] We also observed enhancement in the diode ideality factor (A; 1.45 to 1.17) and reverse saturation current density (Jo; 2.87×10^{-9} to 1.02×10^{-11} $mAcm^{-2}$) (Table 1), which are similar to the reports on CIGS and CZTS material based thin film solar cell devices.[56-58] We speculate that the improvement in the device parameters is due to reduction or mitigation of carrier recombination either at the interfaces or in the bulk of MACl treated perovskite films as a consequence of improved crystallinity, morphology, surface quality as discussed above. V_{OC} and J_{SC} could be improved by further optimization of bulk optoelectronic properties and tuning the charge transport material for better interface quality.[17, 19, 35]

The spectral responses of respective devices are presented in **Figure 6b**. The device with MACl treatment revealed enhanced EQE over a wide wavelength regime (~330-750 nm). The values of J_{SC} calculated by integrating EQE are 18.92 and 17.89 $mAcm^{-2}$ for devices with and without MACl treatment, respectively, which are found to be close to the values obtained from the respective J-V characteristics listed in Table 1. The EQE of PVSCs in longer wavelength

regime, $\lambda > 500$ nm is strongly dependent on quality of perovskite material and interface whereas that of short wavelength regime is strongly influenced by interface layer and interface quality of devices.[18, 59] The IQE [EQE/(1-R)] spectra of devices reached ~80% and ~90% on average in 370-750 nm for respective devices. The reflection of incidence light by the ITO substrate or interface layers of device is one of the limiting factors for further enhancement of photocurrent.[18] Incidentally, we did not apply any antireflection means in this study, hence the additional improvement in EQE is obvious.

Table 1. Photovoltaics parameters/ properties of the encapsulated solar cell devices with perovskite film prepared with and without MACl treatment with device area ~ 0.26 cm^2. J_{SC}: short circuit current density, V_{OC}: open circuit voltage, FF: fill factor, η: power conversion efficiency, R_S: series resistance, R_{Sh}: shunt resistance, A: diode ideality factor, J_0: reverse saturation current density and *: estimated from J-V analysis.

Device	J_{SC} ($mAcm^{-2}$)	V_{OC} (V)	FF	η (%)	R_S ($\Omega \cdot cm^2$)	R_{Sh} ($\Omega \cdot cm^2$)	*A	*Jo ($mAcm^{-2}$)
Without MACl	18.78	0.86	0.77	12.41	4.31	3.58×10^3	1.45	2.87×10^{-9}
with MACl	20.06	0.95	0.79	15.09	4.52	1.70×10^4	1.17	1.02×10^{-11}

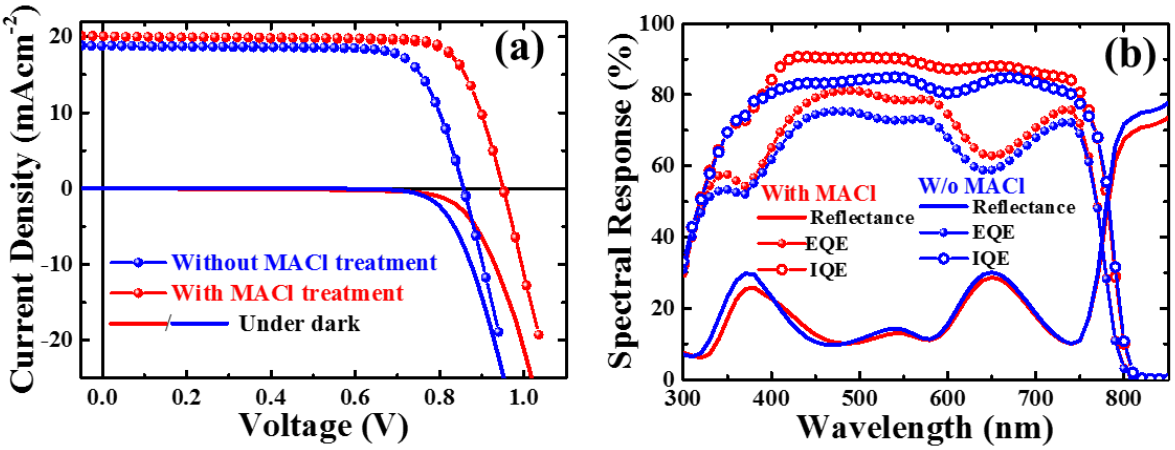

Figure 6. (a) Current density-voltage (J-V) characteristics and (b) spectral response of the perovskite devices with and without MACl treatment.

Furthermore, a comparative study of EQE spectra measured under different bias voltages (Figure S7a, b, supporting information) was performed. In devices without MACl treatment, the EQE spectra under negative bias are much distorted from those under 0V bias. The distortion is better illustrated by taking the ratio, EQE(0V)/EQE($\pm$xV) (Figure S7c, d, supporting information). This is a clear indication of stronger trap assisted recombination[59] in the device without MACl treatment than that in the MACl treated device. We also calculated the band gap energy (E_g) of perovskite layer by differentiating EQE with respect to wavelength vs energy ($\frac{d(EQE)}{d\lambda}$ vs E) (Figure S8). The value (Eg=1.57$\pm$ 0.01 eV) is the same for both types of devices and is close to the value shown by PL spectra. These results support the fact that there are apparent influences on perovskite film quality by MACl treatment but no stoichiometric change, which is consistent with the results of XPS and XRD discussed above.

To elucidate the recombination of photogenerated carriers during device operation, we measured the J-V curves of both types of devices as a function of light intensity as depicted in Figure S9 (supporting information). The light intensity dependence of V_{OC} and J_{SC} can provide information about recombination mechanism under open circuit conditions, where the photogenerated charge carriers recombine within the cell.[60] We analyzed the light intensity dependent V_{OC} given by the relation,[60]

$$V_{OC} = \left(\frac{Ak_BT}{e}\right)\ln(I) + \frac{1}{e}(E_0 - \Delta) \qquad (1)$$

where I is the incident light intensity, A the diode ideality factor, K_B the Boltzmann constant, e elementary charge, T absolute temperature, E_0 the energy gap. A commonly accepted value, $V_{OC} \approx E_0$ is given at T= 0 K and Δ is energy shift of the quasi-Fermi energies within the band gap due to disorder. Figure 7a shows a semilogarithmic plot of V_{OC} as a function of light

intensity and linear fitting. Here the slope of device with MACl treatment is estimated to be ~1.08 k_BT/e, which suggests a bimolecular recombination process dominates during device operation.[60] In contrast, a slope of ~1.45 k_BT/e for the device without MACl treatment indicates the presence of Shockley-Read Hall (SRH) recombination via comparatively deep traps, which act as efficient recombination centers.[50, 60] Furthermore, the light intensity dependence of J_{SC}, $J_{SC} \propto I^{\alpha}$, where the deviation of power factor α from 1 implies bimolecular recombination, were analyzed (**Figure 7**). Figure 7b exhibits the relationship of J_{SC} on light intensity in a double logarithmic scale with slopes of α=0.99 and 0.97 for devices with perovskite films with and without MACl treatment, respectively. The result suggests that contribution of bimolecular recombination loss is rather minor under short circuit conditions in device with MACl treatment.[60-62]

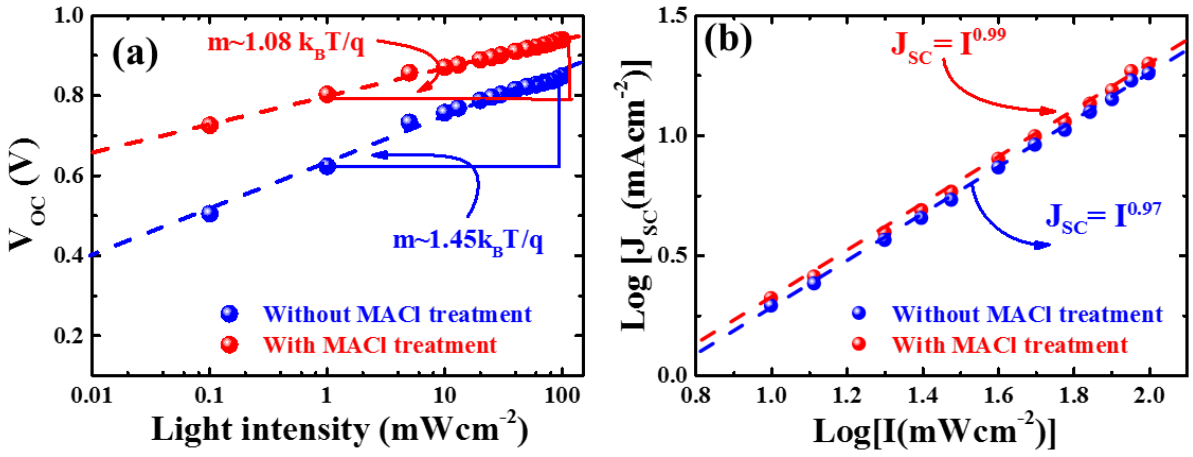

Figure 7. Plots of light intensity dependent V_{OC} (a) and J_{SC} (b) of devices with and without MACl treatment. Here the dashed lines represent linear fit to respective device parameters.

For further confirmation, the electrical properties of devices were extracted by fitting J−V curves according to diode model as described in reports.[57, 63, 64] The plots for estimation of R_S, R_{sh}, J_0, and A are shown in Figure S10 and the deduced data are summarized in Table S1 in supporting information. Good agreement was found between the diode ideality factors

calculated from different approaches and measurements. Other electrical parameters of devices, R_S, R_{Sh}, and G_{Sh} also fall within acceptable range. It is to be noted that the diode ideality factor is associated with the recombination mechanism. The value of A approaching to 1 indicates recombination dominates in the quasi neutral region (QNR) whereas if A approaching to 2, the Shockley-Read-Hall (SRH) recombination mechanism in the space charge region (SCR) is important.[57, 58, 65] In our case, the decrease in A from ~ 1.5 for device without MACl treatment to ~ 1.15 for device with MACl treatment indicates much reduced trap assisted recombination losses in the latter, which is in good agreement with the results from the analysis of the light intensity dependence of V_{OC}. Note also that the reverse saturation current density (J_0) decreases from 2.87×10^{-9} to 1.02×10^{-11} mAcm^{-2} (Table 1 and Table S1) in going from a device without MACl treatment to that with the MACl treatment. J_0 depends on defect activities especially in the absorber layer, which could have strong influence on V_{OC} and FF.[57,64] Therefore, the decrease in J_0 and the improvement in V_{OC} and FF all point to the mitigation of the defect activities in MACl treated devices.

To get a more in-depth understanding on carrier profile, defect level and defect distribution, the devices were investigated by using capacitance spectroscopy (**Figure 8**). We carried out capacitance-voltage (C-V) measurements and extracted the Mott-Schottky plot (Figure 8a) and carrier profile (Figure 8b) estimated by the relation,[65]

$$N_a = -\frac{2}{q\varepsilon_0\varepsilon_s A^2}\left[\frac{d}{dV}\left(\frac{1}{C^2}\right)\right]^{-1} \quad (2)$$

where C is capacitance, ε_0 is permittivity of free space, ε_s is dielectric constant of absorber layer and A is area of device. Both devices were found to be fully depleted, which implies a p-i-n junction with the perovskite layer being an intrinsic semiconductor. These results are in good agreement with other reports.[66,67] The diffusion potential, V_d (given by fermi energy, E_F and built in potential, V_{bi} by $V_d=E_{F/q}-V_{bi}$)[63] is found to be larger for the device with MACl treatment consistent with the higher V_{OC}. The carrier profile (Figure 8b) revealed almost flat

distribution of carrier density ranging from 3.2 - 60× 10^{15} cm^{-3} and the space charge region (SCR) width ~296 nm for the MACl treated device. The untreated device also demonstrated a similar trend of carrier density distribution with slightly higher values ranging from 6.5 - 150× 10^{15} cm^{-3} and the SCR width ~242 nm. The SCR width for MACl treated device is quite large and comparable to thickness of perovskite film, which indicates that the built-in field is comparatively strong, leading to the effective charge extraction and to an efficient device.[66]

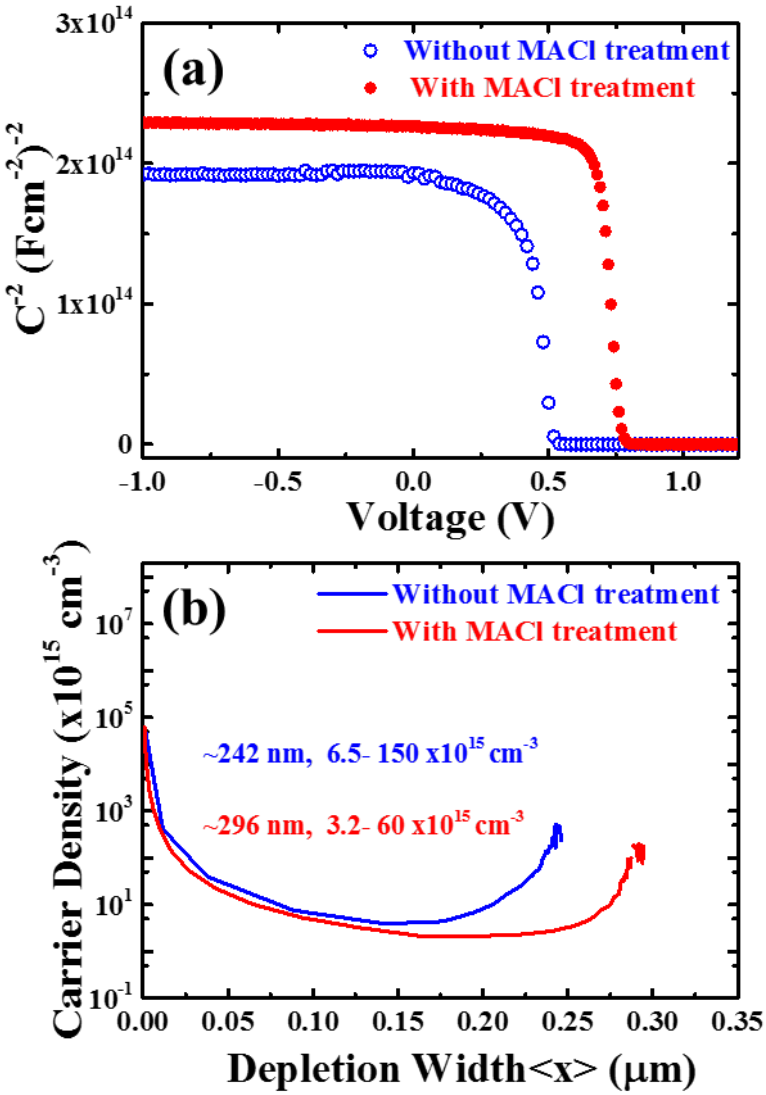

Figure 8. Mott-Schottky plot derived from capacitance - bias voltage (C-V) response of the respective devices (a) and carrier density profiles (b) extracted from the C-V profile. The carrier

density profile range given in plot denotes the minimum carrier density and carrier density close to SCR width.

We further investigated the devices by using admittance spectroscopy (AS) to probe the defect energy level and defect density profile which has been broadly employed in photovoltaic research for defect characterization (**Figure 9**).[65,68-71] The defect states in absorber layer are estimated by employing the Arrhenius plot of characteristic transition frequencies ω_0 expressed by the relation,

$$\omega_0 = 2\upsilon_0 T^2 e^{-E_t/k_B T} \quad (3)$$

where υ_0 is emission factor comprising all the temperature independent parameters and E_t is defect energy level. Similarly, the defect density profile can be derived by the equation,

$$N_t = -\frac{V_{bi}}{ew}\left(\frac{\omega}{k_B T}\frac{dC}{d\omega}\right) \quad (4)$$

Where C is capacitance, V_{bi} is built in potential, w is SCR width, ω is scan frequency and T is absolute temperature. The capacitance-frequency (C-f-T) scans of devices are depicted in Figure 9a, b. Some deviation was observed beyond ~50 kHz frequency which might be due to stronger carrier freeze out. We estimated the dielectric constant of the perovskite films in respective device by evaluating geometric capacitance, $C_g = \frac{\varepsilon A}{t}$, where ε is dielectric constant, A is area and t is thickness of absorber layer as depicted in Figure S11 which was found to be ~ 22 and 25 for devices with and without MACl treatment, respectively, showing good agreement with the report.[64,72] The Arrhenius plots of characteristic frequencies (ω_0), extracted from differentiation of capacitance spectra (Figure S12) are depicted in Figure 9c and the defect distribution in corresponding defect levels are shown in Figure 9d. Note that both devices revealed two defect states. The device without MACl treatment showed two deep trap levels at E'_{t1}~ 0.467 eV and E'_{t2}~ 0.324 eV with emission factors (υ_0), 5.68×10^{11} and

5.76× 10^8 s^{-1}, respectively which are close to the report by Shao et al.[70] The device with MACl treatment demonstrated shallower trap levels at E_{t1}~0.346 eV and E_{t2}~0.241 eV with emission factors (υ_0'), 1.258× 10^{10} and 1.35× 10^8 s^{-1}, respectively, which are in the range reported by Heo et al.[73] The integrated defect densities (Figure 9d) corresponding to the defect levels were found to be in the range of ~10^{17} cm^{-3}, which is comparable to the reports by other groups.[68,70,73] In this analysis, the defect densities were found to be insensitive to the MACl treatment but rather it eliminates deep defects. Deep defects are much more effective in the SRH recombination and hence the trap distribution difference in the MACl treated and untreated devices corroborates well the difference in the respective optoelectronic performance and efficiency.

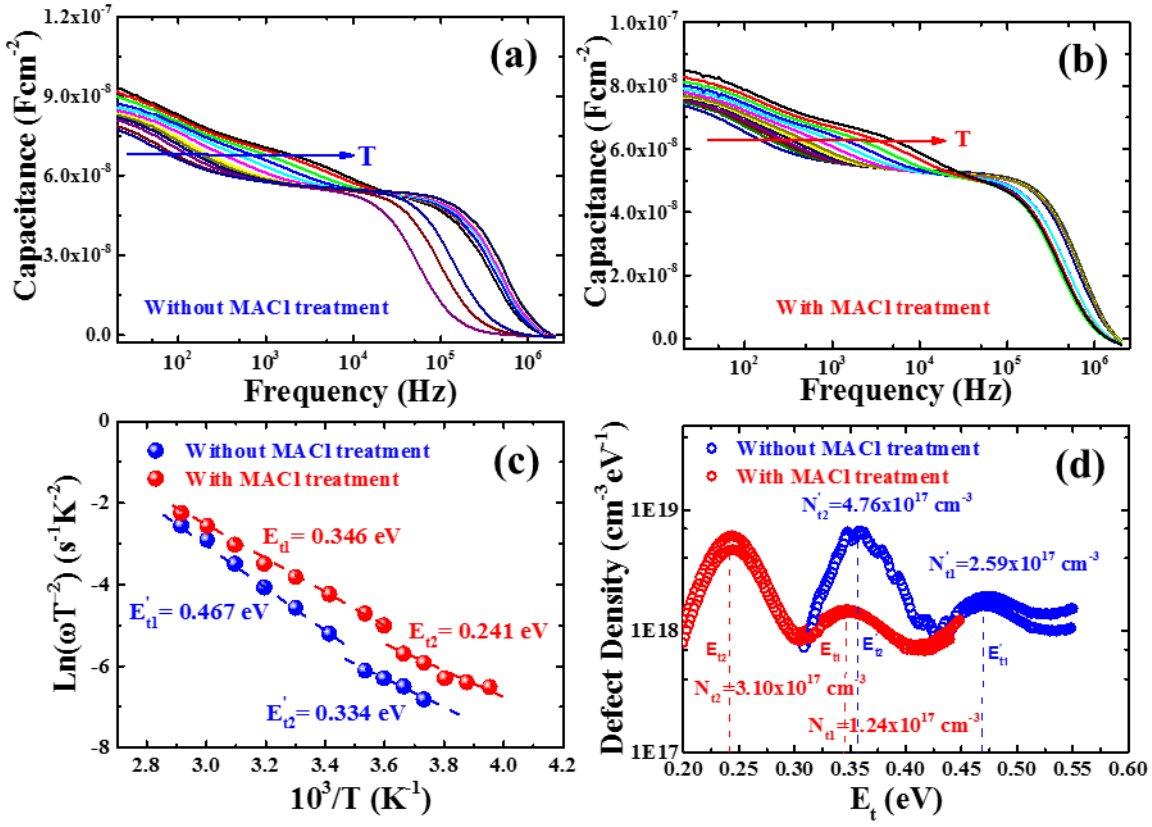

Figure 9. Capacitance frequency (C-f) response of the devices (without and with MACl treatment) (a, b) in the temperature range 243 K to 353 K. The Arrhenius plot (c) and defect distribution profile (d) of respective devices.

Of course, the identification of defect type is quite complicated. One can speculate that the defect levels estimated in our analysis could be related to either of iodine lead antisites (I_{Pb}) and iodine interstitials (I_i) as reported by the density functional theory (DFT).[69,74,75] It is thus quite interesting and challenging to correlate the effect of various fabrication processes with the resulting defect distributions. Only through this endeavor, can one reach a definitive conclusion.

In order to gain better insight into the relationship between the efficiency improvement and observed optoelectronic behavior of devices, we performed device simulation using the program SCAPS (ver. 3.3.01),[76] solar cell capacitance simulator, which is a numerical tool to simulate the impact of properties of layers and interfaces on the device performance.[77,78] Since the perovskite device of planar structure is close to that of typical thin film PV cells, device simulation was carried out adopting the device layers shown in Figure S13 resembling the real device with the layer properties as summarized in Table S2. The simulation was carried out accounting for the material and interface quality by considering the bulk and interface defect density and other layer properties by mimicking experimental results as close as possible. The simulated J-V characteristics demonstrate a good agreement to the general feature of experimental results of respective type of devices as depicted in Figure S14. Although there is slight discrepancy in FF, the simulated device parameters are close enough to experimental results (Table S3). The simulated energy band diagrams of respective type of devices are shown in Figure S15 and are quite similar. In contract, the simulation (Figure S16) showed higher generation current density and lower recombination current density in the MACl treated device, which supports alleviation of defect activities as revealed in the experimental results. The device simulation taking into account the interface and bulk defect profile relating to the layer

quality as depicted in Figure S17 illustrates their impact on J-V characteristics, which conforms to the experimental results.

The fabricated devices were statistically compared by plotting the histograms of device parameters (η, J_{SC}, V_{OC}, FF) as shown in **Figure 10**. The histograms were deduced form 60 devices prepared with or without MACl treatment in 5 batches. The results are summarized in Table 2. The standard deviations of all device parameters for device with MACl treatment are smaller than those without MACl treatment. 80% of devices fabricated with MACl treatment yield PCE of >14% indicating outstanding reproducibility. It is believed that the efficiency can be further improved to a competitive high value[26,34] by addressing some critical issues related to the bulk film quality and introducing more efficient charge transport layers for better optoelectronic properties and carrier dynamics.

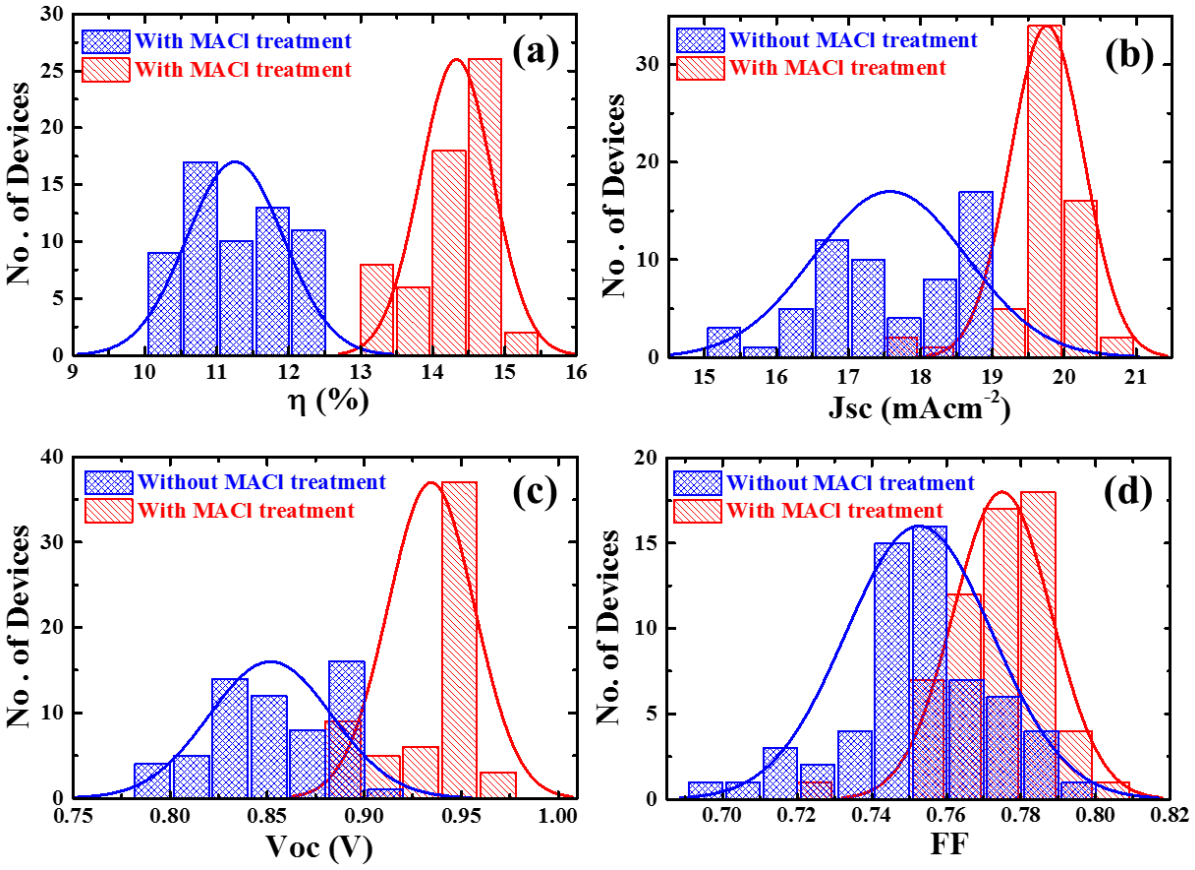

Figure 10. Histogram of device parameters: (a) PEC (η), (b) J_{SC}, (c) V_{OC}, and (d) FF of 60 devices (devices- with and without MACl treatment)

Table 2. Statistics of performance parameters of 60 devices of each methods (perovskite films with and without MACl treatment). Avg: average, Max: maximum, Min: minimum, and STD: standard deviation.

Statistics of devices	without MACl				with MACl			
	J_{SC} ($mAcm^{-2}$)	V_{OC} (V)	FF	η (%)	J_{SC} ($mAcm^{-2}$)	V_{OC} (V)	FF	η (%)
Avg	17.59	0.85	0.75	11.27	19.76	0.93	0.77	14.33
Max	18.96	0.91	0.79	12.41	20.53	0.96	0.80	15.09
Min	15.04	0.78	0.70	10.29	17.52	0.88	0.72	13.34
STD	1.07	0.03	0.02	0.66	0.51	0.02	0.01	0.50

We also monitored the aging effect on performance of encapsulated devices stored in ambient conditions. J-V characteristics of devices were measured periodically as depicted in **Figure 11**. The stability data of more devices are shown in Figure S18 (supporting information). It is observed that there is almost no loss in J_{SC} and FF of both types of devices over the period whereas the device efficiencies decreased slowly after 30 days due to decrease in $V_{OC.}$ The loss in V_{OC} might be caused either by increase in trap centers and defect activities or worsening of interface. The loss in efficiency and V_{OC} is comparatively slower for MACl treated devices. The MACl treated devices retained ~90% of their initial efficiency after 90 days while the devices without the MACl treatment preserved ~80% of their initial efficiency over the same period. These values are comparable to the earlier reports.[27, 50] It is to be noted that hysteresis in JV curve was not observed over the aging time as depicted in Figure S19. This observation

is similar to our earlier report.[50] Even though the origin of hysteresis effect is a matter of strong debate,[23] the hysteresis issue has been well addressed by adjusting the charge transport layer.[4, 70] Moreover, the causes of degradation of our device are not related to the hysteresis either. However, mitigation of defects in bulk and interface, better transport layers, control of ion migration and poor humidity tolerance are still big issues to address for the commercial viability of PVSCs.

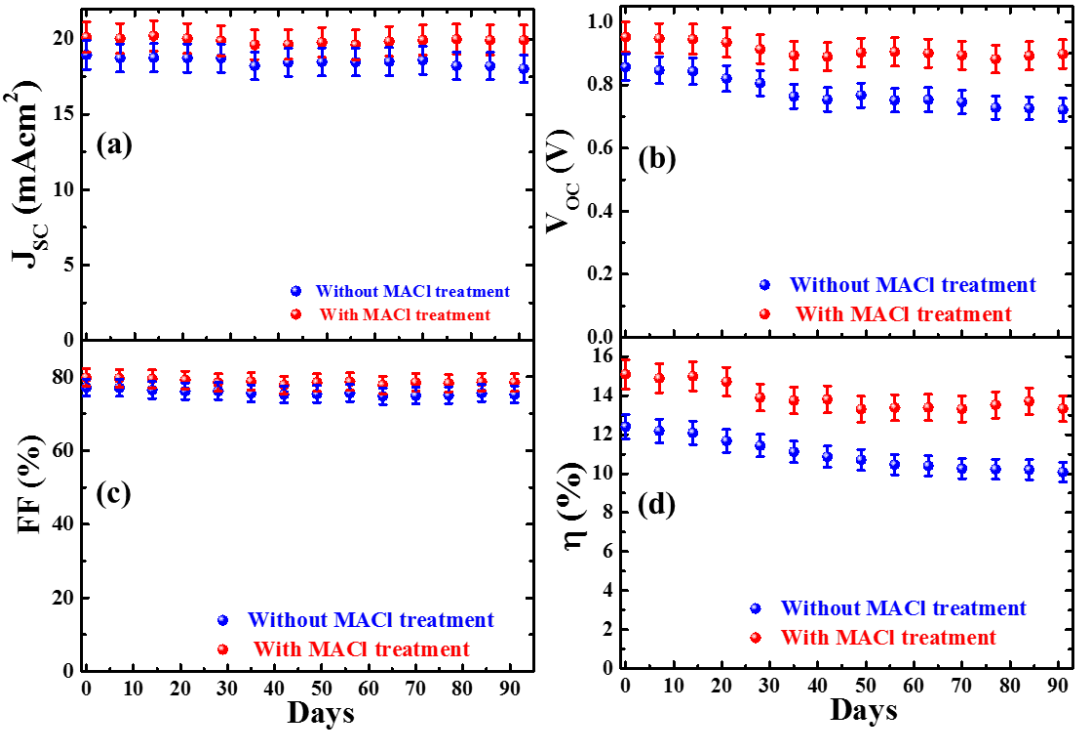

Figure 11. Stability data (solar cell parameters J_{sc}, V_{OC}, FF, and η) of encapsulated devices stored under ambient conditions for 3 months.

3. Conclusion

We report the improvement in device efficiency, stability, and reproducibility of low temperature solution processed planar perovskite device with perovskite thin film annealed in MACl vapor atmosphere. This approach demonstrated better grain morphology and enhanced PL spectra in perovskite thin films. The analysis of device characteristics and capacitance

spectra revealed enhancement in optoelectronic properties with reduction of defect activities and passivation of defect levels, which, we infer, reduce recombination loss. These improvements lead to better device efficiency with reproducibility coupled with promising stability by retaining more than 90% of their initial performance over 60 days. Further progress in device efficiency requires better film and interface quality and defect passivation.

4. Experimental Section

Materials and preparation: All chemicals were purchased from commercial suppliers as mentioned and unless otherwise specified, they were used as received. Methyl ammonium iodide (MAI) and Methyl ammonium chloride (MACl) were of battery grade from Wako chemical company. For the fabrication of perovskite films, precursor solutions were prepared by dissolving PbI_2- DMSO complex (prepared according to literature[17]) in anhydrous DMF (500 mg ml^{-1}), and MAI and MACl in ethanol (50 mg ml^{-1}; 19:1 ratio). [6,6]-Phenyl C_{61} butyric acid methyl ester ($PC_{61}BM$) [Sigma Aldrich, 99% purity] solution (2 wt. %) dissolved in anhydrous chlorobenzene (CB) was used for coating of the electron transport layer (ETL). Tetrabutylamonium iodide (TBAI) (Sigma Aldrich, 99% purity) precursor solution was prepared in ethanol for doping of PCBM surface facing the cathode metal.[79] All the solutions were filtered using 0.45 μm syringe filters to avoid the risk of unwanted particles in the precursor solution.

Device Fabrication: Solar cell devices were fabricated on pre-cleaned patterned indium tin oxide (ITO) coated glass substrates (15 Ω $square^{-1}$). The ITO substrates were pre-cleaned in an ultrasonic bath with detergent, pure water, and 2-propanol, followed by an ultraviolet-ozone treatment for 5 min to remove the organic residuals. A thin HTM layer (30 nm) of poly(3,4-ethylenedioxythiophene):poly(styrene sulfonate) (PEDOT:PSS, Clevios, Al4083) was deposited by spin coating at 3000 rpm and subsequently dried at 130 ℃ for 10 min on a hot

plate in air ambient. Then substrates were transferred into a nitrogen-filled glove box (<1.0 ppm O_2 and H_2O) and the rest of the steps were carried out inside the glove box. PbI_2 precursor solution was spin coated at 3000 rpm for 90 s and a mixed precursor solution of MAI and MACl was subsequently spun on to the PbI_2 layer at 4000 rpm, for 30 s. Then to promote the crystallization, those as grown $CH_3NH_3PbI_{3-x}Cl_x$ perovskite films were simply placed inside the Petri disk with or without MACl powders on hot plate at 100℃ for MACl treatment (Figure S20). We have also maintained the temperature of substrate placed on teflon ring at 100±5 ℃ during annealing of as grown perovskite film under MACl treatment. For ETM layer, $PC_{61}BM$ was spun–coated on top of the perovskite films at 700 rpm for 30 s coupled at 5000 rpm for 10 s, followed by deposition of a thin TBAI layer spinning at 3000 rpm for 25 s. To complete device structure, samples were then transferred into the evaporation chamber connected to the glove box for metal contact deposition. Finally, 100 nm of Ag was thermally evaporated at a pressure $<10^{-4}$ Pa. Devices with area of ~0.26 cm^2 were sealed using UV-curable resins before the subsequent measurements in ambient conditions.

Device Characterizations: The X-ray diffraction (XRD) patterns of fabricated perovskite films were collected using Bruker D8 advanced x-ray diffractometer (CuK_α radiation, λ= 1.54050 A). The morphology of films and cross-sectional images were taken by a high resolution scanning electron microscope (SEM) at 5 kV accelerating voltage (Hitachi, S-4800). The absorption spectra and photoluminescence (PL) spectra of various films were taken using UV-Vis-NIR spectrometer (7200, V-Jasco) and Spectrofluorometer (FP8500, Jasco). The carrier life times were measured with a fluorescence lifetime spectrometer (Quantaurus-τ from Hamamatsu- Photonics K.K.). The current density–voltage (J-V) characteristics and spectral response (incident monochromatic photon to current conversion efficiency (IPCE) spectra, external quantum efficiency (EQE), and reflectance spectra) were characterized with a spectrometer (SM-250IQE, Bunkokeiki, Japan). Capacitance-frequency response (C-f) was

measured with an LCR meter (E4980A, Agilent), which probes from 20 Hz to 2 MHz at ac voltage amplitude of 10 mV under dark condition in the temperature range of 253K−343K whereas capacitance-voltage (C−V) measurements were carried out at 1kHz. For temperature dependent C−f scans, a temperature controlled chamber (SU-221) was used having control system with error of ±0.1K (℃).

Supporting Information

Electronic Supplementary Information is available.

Acknowledgements

The authors acknowledge the support under the MEXT Program for Development of Environment Technology using Nanotechnology.

REFERENCES

1. A. Kojima, K. Teshima, Y. Shirai and T. Miyasaka, *J. Am. Chem. Soc.*, 2009, **131**, 6050-6051.
2. M. A. Green, K. Emery, Y. Hishikawa, W. Warta, E. D. Dunlop, D. H. Levi and A. W. Y. Ho-Baillie, *Progress in Photovoltaics: Research and Applications*, 2017, **25**, 3-13.
3. K. Leo, *Nat Nano*, 2015, **10**, 574-575.
4. M. A. Green, A. Ho-Baillie and H. J. Snaith, *Nat Photon*, 2014, **8**, 506-514.
5. J. H. Heo, S. H. Im, J. H. Noh, T. N. Mandal, C. S. Lim, J. A. Chang, Y. H. Lee, H. J. Kim, A. Sarkar, M. K. Nazeeruddin, M. Gratzel and S. I. Seok, *Nature Photonics*, 2013, **7**, 486-491.
6. A. Miyata, A. Mitioglu, P. Plochocka, O. Portugall, J. T.-W. Wang, S. D. Stranks, H. J. Snaith and R. J. Nicholas, *Nat Phys*, 2015, **11**, 582-587.
7. S. D. Stranks, G. E. Eperon, G. Grancini, C. Menelaou, M. J. P. Alcocer, T. Leijtens, L. M. Herz, A. Petrozza and H. J. Snaith, *Science*, 2013, **342**, 341-344.

8. M. I. Saidaminov, A. L. Abdelhady, B. Murali, E. Alarousu, V. M. Burlakov, W. Peng, I. Dursun, L. Wang, Y. He, G. Maculan, A. Goriely, T. Wu, O. F. Mohammed and O. M. Bakr, *Nat Commun*, 2015, **6**, 7586.
9. W. S. Yang, J. H. Noh, N. J. Jeon, Y. C. Kim, S. Ryu, J. Seo and S. I. Seok, *Science*, 2015, **348**, 1234-1237.
10. Y. Ogomi, A. Morita, S. Tsukamoto, T. Saitho, N. Fujikawa, Q. Shen, T. Toyoda, K. Yoshino, S. S. Pandey, T. L. Ma and S. Hayase, *J Phys Chem Lett*, 2014, **5**, 1004-1011.
11. J. H. Noh, S. H. Im, J. H. Heo, T. N. Mandal and S. I. Seok, *Nano Lett.*, 2013, **13**, 1764-1769.
12. J. Burschka, N. Pellet, S. J. Moon, R. Humphry-Baker, P. Gao, M. K. Nazeeruddin and M. Gratzel, *Nature*, 2013, **499**, 316-319.
13. Y. Deng, Q. Dong, C. Bi, Y. Yuan and J. Huang, *Advanced Energy Materials*, 2016, **6**, 1600372-n/a.
14. M. Z. Liu, M. B. Johnston and H. J. Snaith, *Nature*, 2013, **501**, 395-398.
15. J. You, Z. Hong, Y. Yang, Q. Chen, M. Cai, T.-B. Song, C.-C. Chen, S. Lu, Y. Liu, H. Zhou and Y. Yang, *ACS Nano*, 2014, **8**, 1674-1680.
16. Z. Xiao, C. Bi, Y. Shao, Q. Dong, Q. Wang, Y. Yuan, C. Wang, Y. Gao and J. Huang, *Energ Environ Sci*, 2014, **7**, 2619-2623.
17. N. J. Jeon, J. H. Noh, Y. C. Kim, W. S. Yang, S. Ryu and S. Il Seol, *Nat Mater*, 2014, **13**, 897-903.
18. Z. Xiao, Q. Dong, C. Bi, Y. Shao, Y. Yuan and J. Huang, *Adv. Mater.*, 2014, **26**, 6503-6509.
19. Z. M. Zhou, Z. W. Wang, Y. Y. Zhou, S. P. Pang, D. Wang, H. X. Xu, Z. H. Liu, N. P. Padture and G. L. Cui, *Angew. Chem.-Int. Edit.*, 2015, **54**, 9705-9709.
20. F. Fu, T. Feurer, T. Jäger, E. Avancini, B. Bissig, S. Yoon, S. Buecheler and A. N. Tiwari, *Nat Commun*, 2015, **6**, 8932.
21. C.-C. Chueh, C.-Z. Li and A. K. Y. Jen, *Energ Environ Sci*, 2015, **8**, 1160-1189.
22. J. You, L. Meng, T.-B. Song, T.-F. Guo, Y. Yang, W.-H. Chang, Z. Hong, H. Chen, H. Zhou, Q. Chen, Y. Liu, N. De Marco and Y. Yang, *Nat Nano*, 2016, **11**, 75-81.
23. H. J. Snaith, A. Abate, J. M. Ball, G. E. Eperon, T. Leijtens, N. K. Noel, S. D. Stranks, J. T. W. Wang, K. Wojciechowski and W. Zhang, *J Phys Chem Lett*, 2014, **5**, 1511-1515.
24. K. Miyano, M. Yanagida, N. Tripathi and Y. Shirai, *The Journal of Physical Chemistry Letters*, 2016, DOI: 10.1021/acs.jpclett.6b00579, 2240-2245.

25. D. Wang, M. Wright, N. K. Elumalai and A. Uddin, *Sol. Energy Mater. Sol. Cells*, 2016, **147**, 255-275.
26. J. H. Heo, H. J. Han, D. Kim, T. K. Ahn and S. H. Im, *Energ Environ Sci*, 2015, **8**, 1602-1608.
27. N. Tripathi, M. Yanagida, Y. Shirai, T. Masuda, L. Han and K. Miyano, *Journal of Materials Chemistry A*, 2015, **3**, 12081-12088.
28. Q. Chen, N. De Marco, Y. Yang, T.-B. Song, C.-C. Chen, H. Zhao, Z. Hong, H. Zhou and Y. Yang, *Nano Today*, 2015, **10**, 355-396.
29. G. E. Eperon, V. M. Burlakov, P. Docampo, A. Goriely and H. J. Snaith, *Adv. Funct. Mater.*, 2014, **24**, 151-157.
30. A. Dualeh, N. Tétreault, T. Moehl, P. Gao, M. K. Nazeeruddin and M. Grätzel, *Adv. Funct. Mater.*, 2014, **24**, 3250-3258.
31. Q. Chen, H. P. Zhou, Z. R. Hong, S. Luo, H. S. Duan, H. H. Wang, Y. S. Liu, G. Li and Y. Yang, *J. Am. Chem. Soc.*, 2014, **136**, 622-625.
32. P. Docampo, F. C. Hanusch, S. D. Stranks, M. Döblinger, J. M. Feckl, M. Ehrensperger, N. K. Minar, M. B. Johnston, H. J. Snaith and T. Bein, *Advanced Energy Materials*, 2014, **4**, 1400355-n/a.
33. C.-H. Chiang and C.-G. Wu, *Nat Photon*, 2016, **10**, 196-200.
34. M. Saliba, T. Matsui, J.-Y. Seo, K. Domanski, J.-P. Correa-Baena, M. K. Nazeeruddin, S. M. Zakeeruddin, W. Tress, A. Abate, A. Hagfeldt and M. Grätzel, *Energ Environ Sci*, 2016, **9**, 1989-1997.
35. M. Hu, C. Bi, Y. Yuan, Y. Bai and J. Huang, *Advanced Science*, 2016, **3**, 1500301-n/a.
36. M. D. Xiao, F. Z. Huang, W. C. Huang, Y. Dkhissi, Y. Zhu, J. Etheridge, A. Gray-Weale, U. Bach, Y. B. Cheng and L. Spiccia, *Angew. Chem.-Int. Edit.*, 2014, **53**, 9898-9903.
37. X. Song, W. W. Wang, P. Sun, W. L. Ma and Z. K. Chen, *Appl. Phys. Lett.*, 2015, **106**, 033901.
38. P.-W. Liang, C.-Y. Liao, C.-C. Chueh, F. Zuo, S. T. Williams, X.-K. Xin, J. Lin and A. K. Y. Jen, *Adv. Mater.*, 2014, **26**, 3748-3754.
39. H. B. Kim, H. Choi, J. Jeong, S. Kim, B. Walker, S. Song and J. Y. Kim, *Nanoscale*, 2014, **6**, 6679-6683.
40. W. Zhang, M. Saliba, D. T. Moore, S. K. Pathak, M. T. Horantner, T. Stergiopoulos, S. D. Stranks, G. E. Eperon, J. A. Alexander-Webber, A. Abate, A.

Sadhanala, S. H. Yao, Y. L. Chen, R. H. Friend, L. A. Estroff, U. Wiesner and H. J. Snaith, *Nat Commun*, 2015, **6**.

41. Y. Zhou, M. Yang, W. Wu, A. L. Vasiliev, K. Zhu and N. P. Padture, *Journal of Materials Chemistry A*, 2015, **3**, 8178-8184.
42. H. Yu, X. Liu, Y. Xia, Q. Dong, K. Zhang, Z. Wang, Y. Zhou, B. Song and Y. Li, *Journal of Materials Chemistry A*, 2016, **4**, 321-326.
43. Y. Zhou, M. Yang, O. S. Game, W. Wu, J. Kwun, M. A. Strauss, Y. Yan, J. Huang, K. Zhu and N. P. Padture, *ACS Applied Materials & Interfaces*, 2016, **8**, 2232-2237.
44. E. L. Unger, A. R. Bowring, C. J. Tassone, V. L. Pool, A. Gold-Parker, R. Cheacharoen, K. H. Stone, E. T. Hoke, M. F. Toney and M. D. McGehee, *Chem. Mater.*, 2014, **26**, 7158-7165.
45. A. Dualeh, P. Gao, S. I. Seok, M. K. Nazeeruddin and M. Grätzel, *Chem. Mater.*, 2014, **26**, 6160-6164.
46. M. Yang, Y. Zhou, Y. Zeng, C.-S. Jiang, N. P. Padture and K. Zhu, *Adv. Mater.*, 2015, **27**, 6363-6370.
47. E. Edri, S. Kirmayer, S. Mukhopadhyay, K. Gartsman, G. Hodes and D. Cahen, *Nat Commun*, 2014, **5**, 3461.
48. H. Yu, F. Wang, F. Xie, W. Li, J. Chen and N. Zhao, *Adv. Funct. Mater.*, 2014, **24**, 7102-7108.
49. S. T. Williams, F. Zuo, C. C. Chueh, C. Y. Liao, P. W. Liang and A. K. Y. Jen, *ACS Nano*, 2014, **8**, 10640-10654.
50. N. Tripathi, Y. Shirai, M. Yanagida, A. Karen and K. Miyano, *ACS Applied Materials & Interfaces*, 2016, **8**, 4644-4650.
51. A. L. Patterson, *Physical Review*, 1939, **56**, 978-982.
52. W. Zhang, S. Pathak, N. Sakai, T. Stergiopoulos, P. K. Nayak, N. K. Noel, A. A. Haghighirad, V. M. Burlakov, D. W. deQuilettes, A. Sadhanala, W. Li, L. Wang, D. S. Ginger, R. H. Friend and H. J. Snaith, *Nat Commun*, 2015, **6**, 10030.
53. G. Sadoughi, D. E. Starr, E. Handick, S. D. Stranks, M. Gorgoi, R. G. Wilks, M. Bär and H. J. Snaith, *ACS Applied Materials & Interfaces*, 2015, **7**, 13440-13444.
54. K. Wu, A. Bera, C. Ma, Y. Du, Y. Yang, L. Li and T. Wu, *PCCP*, 2014, **16**, 22476-22481.
55. B. J. Foley, D. L. Marlowe, K. Sun, W. A. Saidi, L. Scudiero, M. C. Gupta and J. J. Choi, *Appl. Phys. Lett.*, 2015, **106**, 243904.

56. W. Wang, M. T. Winkler, O. Gunawan, T. Gokmen, T. K. Todorov, Y. Zhu and D. B. Mitzi, *Advanced Energy Materials*, 2014, **4**, 1301465-n/a.
57. D. B. Khadka, S. Kim and J. Kim, *The Journal of Physical Chemistry C*, 2016, **120**, 4251-4258.
58. T. Gershon, T. Gokmen, O. Gunawan, R. Haight, S. Guha and B. Shin, *MRS Communications*, 2014, **4**, 159-170.
59. Q. Lin, A. Armin, R. C. R. Nagiri, P. L. Burn and P. Meredith, *Nat Photon*, 2015, **9**, 106-112.
60. S. R. Cowan, A. Roy and A. J. Heeger, *Physical Review B*, 2010, **82**, 245207.
61. V. V. Brus, C. M. Proctor, N. A. Ran and T.-Q. Nguyen, *Advanced Energy Materials*, 2016, **6**, 1502250-n/a.
62. M. Jahandar, J. H. Heo, C. E. Song, K.-J. Kong, W. S. Shin, J.-C. Lee, S. H. Im and S.-J. Moon, *Nano Energy*, 2016, **27**, 330-339.
63. S. S. Hegedus and W. N. Shafarman, *Progress in Photovoltaics: Research and Applications*, 2004, **12**, 155-176.
64. K. Miyano, M. Yanagida, N. Tripathi and Y. Shirai, *Appl. Phys. Lett.*, 2015, **106**, 093903.
65. J. Heath and P. Zabierowski, in *Advanced Characterization Techniques for Thin Film Solar Cells*, Wiley-VCH Verlag GmbH & Co. KGaA, 2011, DOI: 10.1002/9783527636280.ch4, pp. 81-105.
66. H. Tsai, W. Nie, J.-C. Blancon, C. C. Stoumpos, R. Asadpour, B. Harutyunyan, A. J. Neukirch, R. Verduzco, J. J. Crochet, S. Tretiak, L. Pedesseau, J. Even, M. A. Alam, G. Gupta, J. Lou, P. M. Ajayan, M. J. Bedzyk, M. G. Kanatzidis and A. D. Mohite, *Nature*, 2016, **doi:10.1038/nature18306**.
67. K. Miyano, N. Tripathi, M. Yanagida and Y. Shirai, *Acc. Chem. Res.*, 2016, **49**, 303-310.
68. H.-S. Duan, H. Zhou, Q. Chen, P. Sun, S. Luo, T.-B. Song, B. Bob and Y. Yang, *PCCP*, 2015, **17**, 112-116.
69. W.-J. Yin, J.-H. Yang, J. Kang, Y. Yan and S.-H. Wei, *Journal of Materials Chemistry A*, 2015, **3**, 8926-8942.
70. Y. Shao, Z. Xiao, C. Bi, Y. Yuan and J. Huang, *Nat Commun*, 2014, **5**, 5784.
71. D. B. Khadka, S. Kim and J. Kim, *The Journal of Physical Chemistry C*, 2015, **119**, 12226-12235.
72. I. Zarazua, J. Bisquert and G. Garcia-Belmonte, *The Journal of Physical Chemistry Letters*, 2016, **7**, 525-528.

73. J. H. Heo, D. H. Song, H. J. Han, S. Y. Kim, J. H. Kim, D. Kim, H. W. Shin, T. K. Ahn, C. Wolf, T.-W. Lee and S. H. Im, *Adv. Mater.*, 2015, **27**, 3424-3430.
74. M. H. Du, *Journal of Materials Chemistry A*, 2014, **2**, 9091-9098.
75. J. M. Azpiroz, E. Mosconi, J. Bisquert and F. De Angelis, *Energ Environ Sci*, 2015, **8**, 2118-2127.
76. M. Burgelman, P. Nollet and S. Degrave, *Thin Solid Films*, 2000, **361–362**, 527-532.
77. J. Pettersson, M. Edoff and C. Platzer-Björkman, *J. Appl. Phys.*, 2012, **111**, 014509.
78. A. Chirilă, S. Buecheler, F. Pianezzi, P. Bloesch, C. Gretener, A. R. Uhl, C. Fella, L. Kranz, J. Perrenoud, S. Seyrling, R. Verma, S. Nishiwaki, Y. E. Romanyuk, G. Bilger and A. N. Tiwari, *Nat Mater*, 2011, **10**, 857-861.
79. C. Z. Li, C. C. Chueh, F. Z. Ding, H. L. Yip, P. W. Liang, X. S. Li and A. K. Y. Jen, *Adv. Mater.*, 2013, **25**, 4425-4430.

Table of Contents Graphics